The Visualization of Diffusion Tensor Fields in the Brain

Burkhard Wünsche and Richard Lobb
Department of Computer Science
The University of Auckland, Private Bag 92019
Auckland, New Zealand
Email: {burkhard,richard}@cs.auckland.ac.nz

Abstract— **Diffusion Tensor Imaging (DTI) is a relatively new image modality which can be used to gain in vivo information about the anatomy of the brain. We have developed a visualization workbench for the analysis of tensor fields in biological tissue and will describe an incremental approach for the exploration of diffusion tensor data. Our approach starts with slice images familiar to the medical specialist and progressively expands the dimension and abstraction level of the representation in order to provide new insight into the data. In particular we present two new techniques for the visualization of DTI data: Barycentric colour maps allow an integrated view of different types of diffusion anisotropy. Transparency modulated Line Integral Convolution creates an image segmented by tissue type and incorporating a texture representing the 3D orientation of nerve fibers. The quality of our exploration approach and new visualization techniques is demonstrated by identifying various anatomical structures and features in a diffusion tensor data set of a healthy brain.**

Key Words: Visualization - tensor fields - diffusion tensor imaging - brain anatomy

Note: The colour images used in this paper are available at `http://www.cs.auckland.ac.nz/~bwue001/PhD/METMBS/metmbs.html`

I. Introduction

One recent advance in medical imaging has been the introduction of diffusion tensor imaging (DTI) which allows the measurement of water diffusion in the brain [1]. The diffusion tensor describes the spatial distribution of water molecules originating at a common location. Since the diffusion of water depends on the micro-structure of the tissue, visualizing the diffusion tensor field improves the understanding of the anatomy and the physiology of the brain. The results can be used in surgical planning, cognitive sciences [19], and the diagnosis and treatment of various white and gray matter disorders [18], [10], [11], [20]. Visualizing the nerve fiber structure also represents a valuable teaching tool.

We have developed a visualization workbench which allows the user to experiment with various old and new tensor visualization techniques. Combining various tensor visualization techniques with new functionalities provided by our workbench provides new insight into diffusion tensor data.

In this paper we first give an introduction to diffusion tensor imaging and review previous visualization efforts. It follows an overview of our visualization workbench. In the remainder of the paper we use the capabilities of our workbench in order to systematically explore diffusion tensor data. Starting with 2D slice images traditionally used by medical specialists we incrementally increase the complexity of the representation until we obtain a 3D representation of nerve fiber tracts. In addition two novel techniques are presented which give an integrated view of diffusion anisotropy types, provide a visual segmentation of tissue types, and represent the 3D orientation of nerve fiber tracts.

II. Diffusion Tensor Imaging

Diffusion tensor imaging (DTI) is used to measure the intrinsic properties of water diffusion in the brain by an orientation invariant quantity, the diffusion tensor $\mathbf{D}$ [18]. This is possible since the spatial distribution of water molecules originating at a point location after an infinitesimal time period is described by an ellipsoid. The lengths and orientations of the principal axes of this diffusion ellipsoid are given by the eigenvalues λ_i and eigenvectors $\mathbf{v}_i$ ($i = 1, \ldots, 3$), respectively, of the symmetric second-order tensor $\mathbf{D}$ which is represented by a symmetric 3×3 matrix. We use the convention that $\lambda_1 \geq \lambda_2 \geq \lambda_3$, i.e., λ_1 indicates the maximum diffusivity.

DTI uses diffusion weighted MR imaging (DWI) and almost completely suppresses water in blood vessels [Peter Basser, May 2000, private communication]. It therefore measures the diffusion of cerebral spinal fluid (CSF) and fluid within the tissue. The results of the measurement are the six components of the symmetric diffusion tensor $\mathbf{D}$ and the T_2 weighted signal intensity in the absence of diffusion sensitization. Images of water diffusion can provide pathophysiological information complementary to T_1 and T_2 weighted MRI images. The technique is sensitive to movements of the order of a few microns and is described in more detail in [1], [18].

In the brain DTI can be used to differentiate two types of structures. Fluid filled compartments are characterized by a very high *isotropic* diffusion, i.e., the diffusion is similar in all directions. In contrast *white matter* consists of nerve fibers which restrict the diffusion to one direction only due to the presence of cell membranes and myelin sheaths surrounding the axons. Fiber tracts, consisting of parallel nerve fibers, are therefore identified as areas of a high anisotropic diffusion. The orientation of such fiber tracts is determined from the principal directions (eigenvectors) of the diffusion tensor. Finally *gray matter* con-

sists of neural cell bodies, support cells, intermingling nerve fibers and connecting contacts, and is characterized by a low, isotropic diffusion.

Introducing scalar measures for the above diffusion properties makes it possible to gain in vivo information about the anatomy, microstructure and physiology of the brain. A high isotropic diffusion can be measured by the *mean diffusivity* [1] which is defined as the average eigenvalue of the diffusion tensor and is efficiently computed by using the first tensor invariant [14]

$$\lambda_{mean} = \frac{\lambda_1 + \lambda_2 + \lambda_3}{3} = \frac{D_{11} + D_{22} + D_{33}}{3} \quad (1)$$

The diffusion anisotropy is measured by [2], [4]

$$\lambda_{anisotropy} = ((\mathbf{D} - \lambda_{mean}\mathbf{I})^T(\mathbf{D} - \lambda_{mean}\mathbf{I}))/\lambda_{mean}^2 \quad (2)$$

Note that both expressions can be efficiently calculated without computing the eigenvalues and eigenvectors.

Alternative measures have been proposed by Westin et al. [23]. The authors define a *linear isotropy* λ_l, a *planar isotropy* λ_p, and an *isotropy* λ_s as

$$\lambda_l = \frac{\lambda_1 - \lambda_2}{\lambda_1 + \lambda_2 + \lambda_3} \quad (3)$$

$$\lambda_p = \frac{2(\lambda_2 - \lambda_3)}{\lambda_1 + \lambda_2 + \lambda_3} \quad (4)$$

$$\lambda_s = \frac{3\lambda_3}{\lambda_1 + \lambda_2 + \lambda_3} \quad (5)$$

The measures fall in the range $[0, 1]$ and sum up to 1 and define therefore a barycentric space of anisotropies.

III. Previous Work

Traditionally work in DTI has concentrated on the statistical evaluation and the segmentation of the data and their correlation with anatomical features. Pierpaoli et al. [18], for example, use statistical voxel based methods to identify regions of anisotropy, oblate anisotropy, cylindrical anisotropy and asymmetric anisotropy and determine the significance of differences in these measures between various white matter regions. They further use the mean diffusivity and diffusion anisotropy to segment MRI slices into white matter, gray matter and CSF.

Diffusion tensors in the medical field have been traditionally visualized in two dimensions, usually by representing a derived scalar measure over a grid plane with a colour map or a gray scale map. More advanced visualization techniques representing higher level information have been proposed recently. Westin et al. [22] present image processing methods for smoothing tensor data and tracking nerve fiber directions. Poupon et al. [19] track white matter fibers using a Markovian model and the assumption that fiber tracks can not end in white matter. The principal diffusion direction and the extracted nerve fibers are visualized using small normalised cylinders. Basser et al. [3] first reconstruct a continous diffusion tensor field and then employ a high-order streamline integrator to compute fiber tracts. The fiber tracts are represented as shaded surface and by using a maximum intensity projection. Weinstein et al. [21] track white matter fiber tracts using an advection-diffusion model which is claimed to give better results in regions of local complexity where the diffusion tensor data is influenced by multiple features.

Full tensor information has been represented using diffusion ellipsoids and concepts from oil painting [15]. Kindlmann and Weinstein [13] visualize the 3D geometry of the diffusion tensor field using a direct volume rendering technique with the color, lighting and opacity assignment governed by the underlying tensor field. The resulting images resemble the ones obtained by standard volume visualization but contain additional information represented by the colour and the illumination. The main drawbacks are the difficulty in discerning edges due to the illumination definition and the lack of interactivity as a consequence of the slow rendering.

Zhang et al. [27] introduce streamtubes and streamsurfaces for DTI. The trajectory of a streamtube follows the maximum diffusion direction whereas its ellipsoidal cross section represents the medium and minimum diffusivities. The authors normalize the cross section so that it has a constant maximum diameter and its aspect ratio reflects the ratio of the transverse diffusivities. Streamtubes are initially constructed for each voxel exceeding an anisotropy threshold and are then culled to a representative subset taking into account length, average anisotropy and similarity to neighbouring streamlines. Streamsurfaces identify structures where diffusion occurs predominantly within a plane and are computed as an integral surface perpendicular to the minimum diffusion direction.

IV. The Visualization Workbench

We have developed a visualization workbench for the analysis and display of tensor fields in biological tissue [26], [25]. The main features of the workbench are its modular structure, an object-oriented flexible field data structure, advanced colour mapping capabilities, and tools for the selection and filtering of sample points. A visualization is generated by creating for a model a visualization object which is rendered in a window using a view control. The view control contains view parameters including model position and orientation, lighting information, and viewing tools such as clipping planes and mirrors. Models, visualization objects, view controls, and windows are separate objects which can be connected in various ways. As a result it is possible to create different visualizations for the same model, display the same visualization in different windows using different views or to compare different models using the same view. The feature proved useful when comparing the strain tensor field in a sick and a healthy heart [25].

The object-oriented field data structure allows a grid-independent representation of different fields. As a result analytically defined fields and fields defined over different grids can be compared giving the scientist increased capabilities for the exploration and comparison of data sets. Furthermore new fields such as eigenvalue, eigenvector, vec-

tor magnitude, tensor component and gradient fields can be easily derived using predefined operators.

Colour maps are a popular tool for the visualization of scalar fields. Our workbench gives the user increased freedom in the definition of colour maps as is demonstrated in the next section. Defining the colour map control as an independent module makes it possible to use the same colour map for different fields of different models.

The selection and filter tools for sample points are most frequently employed for the placement of visualization icons. Sample points can be selected in world or material coordinates over a 2D or 3D subspace of the model.

V. Exploration of a Diffusion Tensor Data Set

This sections presents a step-by-step exploration of diffusion tensor data starting with simple slice images and culminating with complex 3D representations of nerve fiber tracts.

A. Colour Mapped Surfaces

Traditionally MRI data is displayed as a set of slices parallel to one of the coordinate planes. As an example consider figure 1 which shows four equidistant horizontal slices through the middle section of the brain (from top to bottom) colour mapped with the maximum diffusivity λ_1 (top row), the mean diffusivity λ_{mean} (middle row) and the diffusion anisotropy $\lambda_{anisotropy}$ (bottom row), respectively.

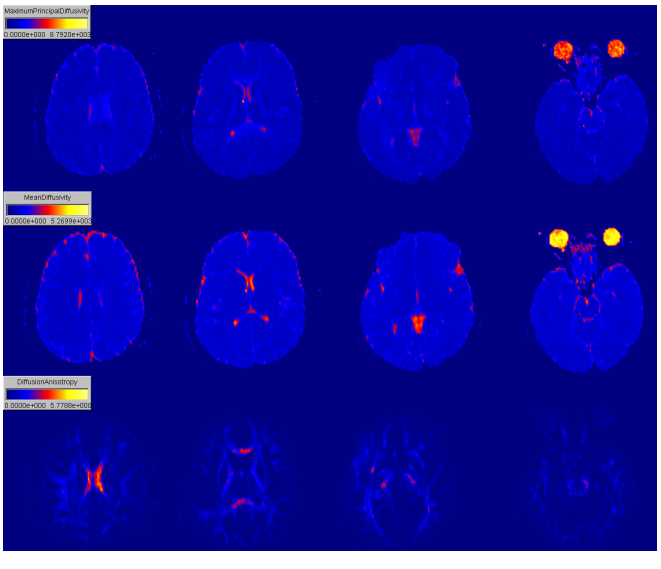

Fig. 1. Horizontal maps of the maximum diffusivity (top row), mean diffusivity (middle row) and diffusion anisotropy (bottom row).

Using simple colour maps allows a medical specialist to identify structures. However, the task is difficult because of low contrast and much detail is obscured. It has been shown that in general a simple gray scale map is better suited for feature identification than using standard colour maps [16].

B. Advanced Colour Mapping

More structures can be identified by scaling the colour map exponentially as done in the left hand side of figure 2. The dark blue coloured region enclosed by the corpus callosum and the internal capsule represents the thalamus and the lateral ventricle. The yellow dot in its centre is the fornix. The anisotropic regions in the periphery of the brain are due to eddy currents induced in the gradient/magnet system during DTI [18].

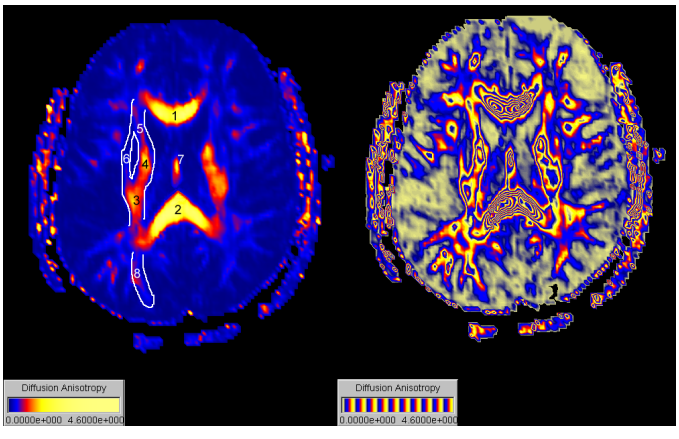

Fig. 2. Horizontal slice with the diffusion anisotropy visualized using an exponential (left) and a cyclical colour map (right). The following white matter structures are indicated by numbers: Genu (1) and splenium (2) of the corpus callosum, genu (4), anterior limb (5) and posterior limb (3) limb of the internal capsule, external capsule (6), fornix (7), and optic radiation (8).

A cyclical colour map with many cycles can be used to displays isocontours of constant diffusion anisotropy as shown in the right hand side of figure 2. Furthermore the density of different isocontours indicates the gradient of the diffusion anisotropy. It is interesting to note that when comparing the isocontours in white matter regions on the left and right hand side of the image the anisotropy is almost symmetric in the anterior side of the brain (the top of the figure) but is slightly asymmetric at the posterior side with higher values for the left hemisphere. This result seems to be in contrast to findings by [17] but is consistent with the fact that the left hemisphere contains an additional brain region responsible for verbal abilities. One hypothesis is that the white matter regions in the left hemisphere are more compact and therefore the fibers are more aligned. It would be interesting to see whether similar results are obtained by examining additional data sets.

As a new visualization technique we propose a barycentric colour map which visualizes linear anisotropic, planar anisotropic, and isotropic diffusion as defined in equations 3–5. The technique makes use of the fact that barycentric coordinates define a point in a triangle where at each vertex of the triangle one of the coordinates is one and the other coordinates are zero. A point in the tensor field can therefore be associated with a colour by defining a triangular colour map as done in figure 3 and determining its colour at the barycentric coordinates $(\lambda_l, \lambda_p, \lambda_s)$.

Figure 3 shows that the diffusion is predominantly linear in the genu and splenium of the corpus callosum and the internal capsule indicating a high alignment of fibers. Planar diffusion is found in the optic radiation and some peripheral white matter regions possibly indicating a crossing of fiber tracts.

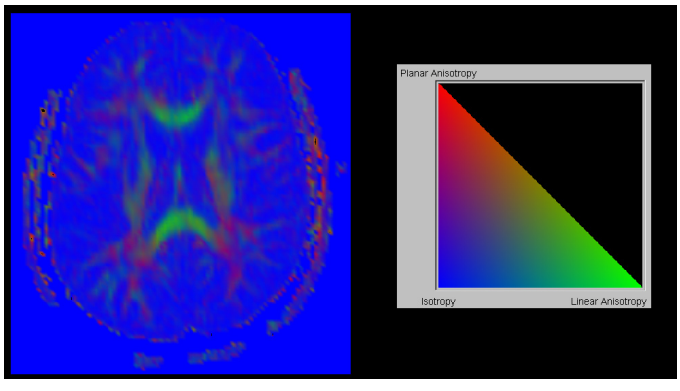

Fig. 3. Barycentric colour map visualizing regions of isotropic, linear anisotropic and oblate anisotropic diffusion

C. Tensor Ellipsoids

Colour mapped slices display only scalar information. In the next stage of the exploration we represent slices in three-dimensional space and add 3D icons in order to uncover directional information. This is achieved by overlaying a slice image with tensor ellipsoids the major axis of which indicate the principal diffusion directions. Using tensor ellipsoids can result in visual cluttering, especially when the tensor size varies largely as is the case when comparing gray matter and CSF. Laidlaw et al. [15] solve this problem by normalise the ellipsoids such that their largest radii are equal. A better visual result is obtained by creating ellipsoids in white matter regions only. This can be easily accomplished by using the filter tool of our workbench.

Figure 4 shows a sagittal slice colour mapped with the mean diffusivity and overlayed with tensor ellipsoids. A filter is employed and ellipsoids are only displayed in white matter regions characterized by $\lambda_{mean} \leq 1250{*}10^{-6} mm/sec$ and $\lambda_{anisotropy} \geq 0.2$. The image on the left hand side represents an enlargement of the section indicated by the white rectangle in the top image. The image on the right hand side shows the same slice tilted by about 45 degree. Fluid filled compartments are indicated by red, orange and yellow colours (4,5). Strongly aligned fibers are revealed by long thin ellipsoids. The fiber direction in the fornix (2) is parallel to the image plane whereas the corpus callosum (the arc shaped region stretching form (1) to (3)) has fibers orthogonal to the image plane. Note that the ellipsoids in the genu (1) and splenium (3) of the corpus callosum are extremely flat and that the anisotropy in these regions reaches a maximum. This observation is consistent with the horizontal map of the anisotropy (figure 2).

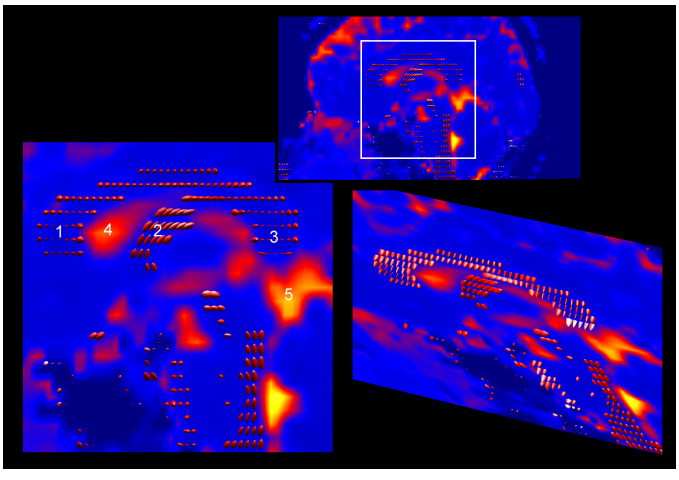

Fig. 4. Saggital section colour mapped with the mean diffusivity and overlayed with diffusion ellipsoids at the MRI grid vertices: 1-genu of corpus callosum, 2-fornix, 3-splenium of corpus callosum, 4-lateral ventricle, 5-fourth ventricle.

D. Transparency Modulated Line Integral Convolution

As an improved visualization method for fiber direction in slice images we propose *transparency modulated Line Integral Convolution*. Line Integral Convolution (LIC) has been originally proposed by Cabral and Leedom as a method to visualize vector fields by convolving a noise texture with the field [5]. We use the principal diffusion direction as a vector field but additionally define transparency values inversely proportional to the diffusion anisotropy in order to remove regions not corresponding to white matter. The resulting texture is then blended with a colour mapped image of the mean diffusivity using the OpenGL "GL_BLEND" operation [24]. The three dimensional direction of a nerve fiber is encoded by varying the length of a convolution kernel with the normal component of the principal diffusion direction. Additional details are found in [25].

Using this technique the colour coding of the resulting image provides a segmentation by tissue type as demonstrated in figure 5. The cyan and green regions represent areas of high mean diffusivity and low anisotropy and therefore indicate fluid filled compartments. The whitish regions represent areas of low anisotropy and low mean diffusivity and therefore indicate gray matter. Textured regions exhibit a high anisotropy and indicate white matter. Very long texture components indicate fiber tracts parallel to the image plane, e.g., the splenium of the corpus callosum (2). In contrast a noise-like texture with very short texture components indicates fiber tracts almost orthogonal to the image plane, e.g., the external capsule (1).

E. Streamtubes

As explained in the previous sections nerve fibers are characterized by a high anisotropic diffusion with directional information given by the principal diffusion direction. Fiber tracts can therefore be extracted by integrating in the direction of the maximum diffusivity in regions

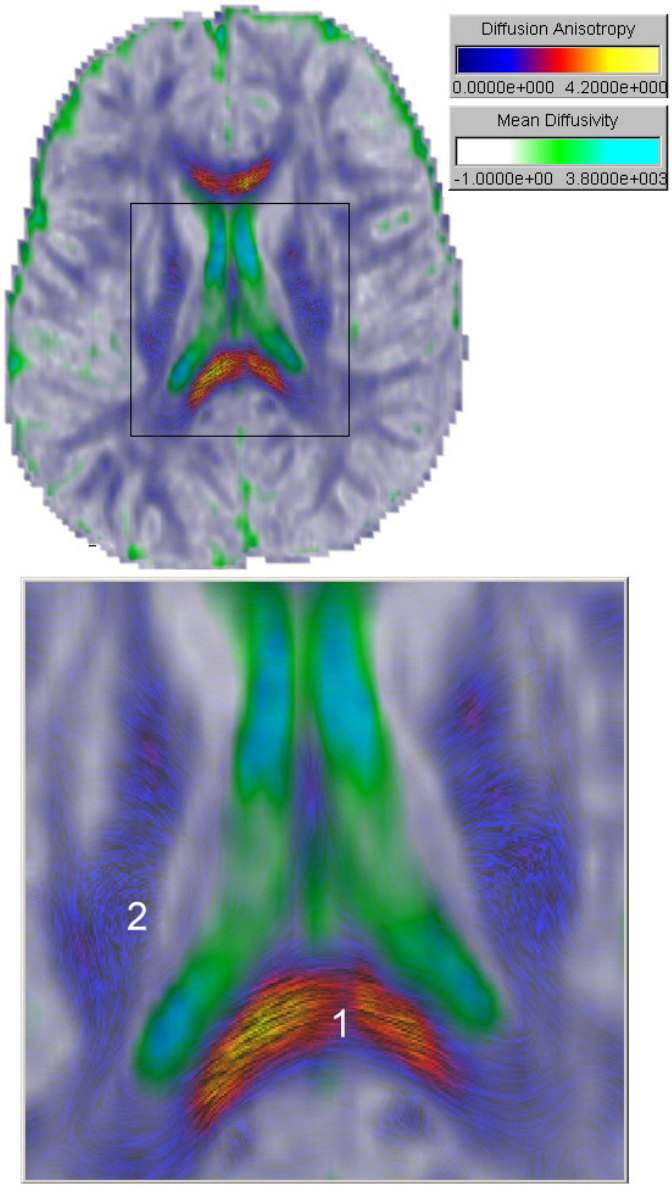

Fig. 5. Fiber tract direction over a horizontal slice through the brain visualized using transparency modulated LIC. The nerve fibers in the splenium of the corpus callosum are parallel to the image plane (2) whereas nerve fibers in the external capsule (1) are almost vertical to it.

of high diffusion anisotropy. Since similar diffusion properties can occur due to noise or eddy currents the maximum diffusivity at any step during the streamline integration must exceed a certain predefined minimum value and the streamline must exceed a specified minimum length.

Figure 6 was created by using start points for streamline integration with $\lambda_{anisotropy} \geq 0.7$ and $\lambda_1 \geq 1000 * 10^{-6} mm/s$ and an integration condition of $\lambda_{anisotropy} \geq 0.3$ and $\lambda_1 \geq 750 * 10^{-6} mm/s$. In order to obtain a dense image $2 \times 2 \times 2$ start points per voxel of the raw MRI data were chosen. Perception of the 3D geometry of line segments is difficult since depth cues due to shading or occlusion are missing. We therefore generate streamtubes by fitting a cylinder with constant radius around each streamline. In order to reduce complexity the maximum number of streamtubes intersecting a voxel is limited to eight.

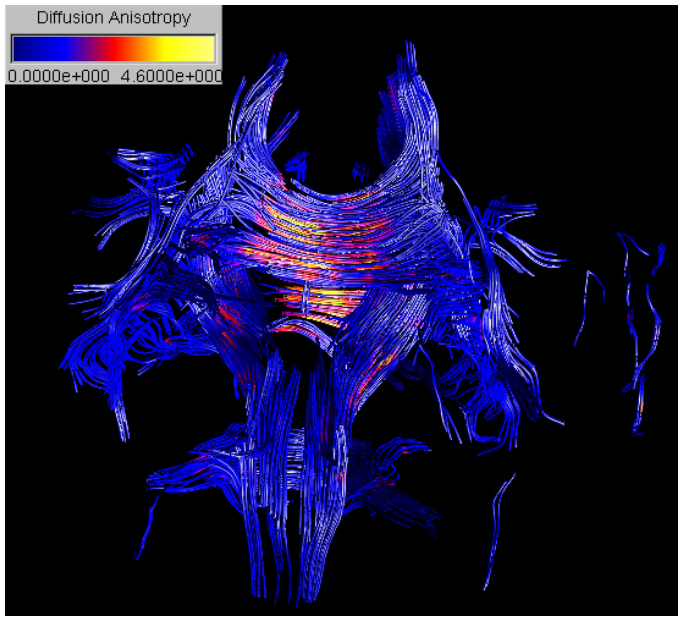

Fig. 6. Fiber tracts visualized using cylindrical streamtubes colour mapped with the diffusion anisotropy.

F. *Hyperstreamlines*

Streamlines and streamtubes contain only information about the major diffusion direction. An improvement is achieved by using hyperstreamlines [6] whose cross section represents the transverse diffusion in fiber tracts. If the hyperstreamline's diameters vary greatly this can lead to visual cluttering. Zhang et al. therefore normalise the hyperstreamlines such that the maximum diameter is constant [27]. Our results show that this is unnecessary and leads to the loss of useful information.

Figure 7 shows the nerve fiber tracts in the brain visualized with hyperstreamlines. The image shows from left to right and top to bottom the left lateral, posterior, superior and anterior side of the brain. The images were generated using one start point per voxel with a start point condition of $\lambda_{anisotropy} \geq 0.7$ and $\lambda_1 \geq 1000$ and an integration condition of $\lambda_{anisotropy} \geq 0.3$ and $\lambda_1 \geq 750$. The minimum length of a streamline was $35mm$ with only one streamline per cell being allowed. The hyperstreamlines were colour mapped with the maximum diffusivity. Comparing the images with photographs and drawings from the literature [7], [8], [9], [12] various fiber tracts can be identified. The classifications were subsequently confirmed by consulting a neuroanatomist and are displayed in the caption of figure 7. In order to improve the perception of the 3D anatomy the eyes and ventricles were extracted as isosurface of the mean diffusivity and added to the scene as green and red surfaces, respectively.

Care has to be take when interpreting hyperstreamline images. In particular fiber tracts might not be represented

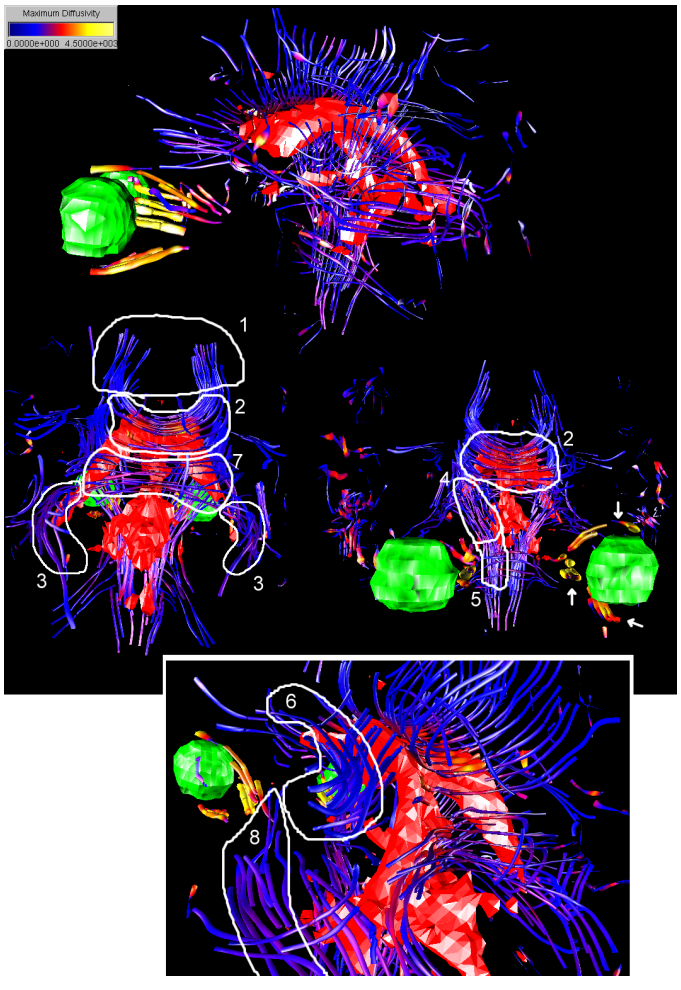

Fig. 7. Hyperstreamlines colour mapped with the maximum diffusivity: 1-Corona radiata, 2-Corpus callosum, 3-Optic radiation, 4-Internal capsule, 5-Cerebral peduncles, 6-Superior longitudinal fasciculus, 7-Splenium of the corpus callosum, 8-Inferior occipito-frontal fasciculus.

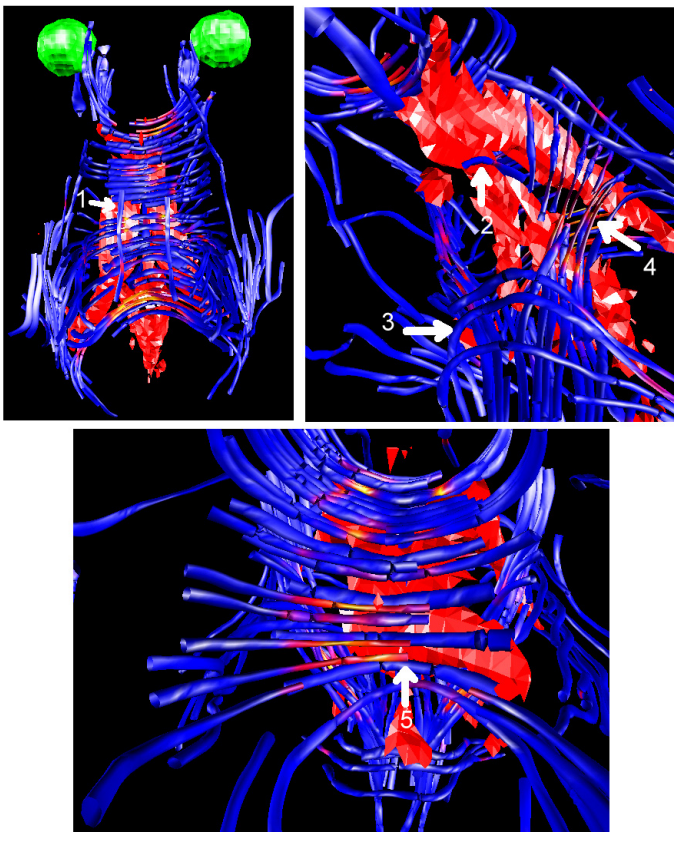

Fig. 8. Close up views of a visualization of fiber tracts using hyperstreamlines colour coded with the diffusion anisotropy: 1-cingulum, 2-fornix, 3-middle cerebellar peduncle, 4-posterior limb of the internal capsule, 5-splenium of the corpus callosum.

at all or are represented by multiple streamlines making it difficult to distinguish separate tracts. As an example consider the three groups of hyperstreamlines close to the eyeball indicated in figure 7 by arrows. The arrow in the middle indicates the *optic nerve* whereas the top and bottom arrow indicate the *opthalmic division* and the *maxilliary division* of the *trigeminal nerve* (cranial nerve V), which conducts sensory impulses from the cornea and the skin. The *oculomotor nerve*, which controls the eye muscle, is not visible presumably because of its relatively small diameter. Note that even though the diameter of the other nerves is relatively small they are represented by several hyperstreamlines each. Possible reasons are the limited resolution of the DTI data, branching of the nerves close to the retina and the presence of the ciliary ganglion. It is also interesting to note that the maximum diffusivity of white matter in the optic nerve considerably higher than in most other white matter regions except for some parts of the corpus callosum.

In order to better differentiate features stricter conditions for the definition of hyperstreamlines can be enforced. Figure 8 shows a posterior, superior, and posterior left lateral view of a visualization obtained using one start point per cell with a start point condition of $\lambda_{anisotropy} \geq 1.0$ and $\lambda_1 \geq 1000$ and an integration condition of $\lambda_{anisotropy} \geq 0.3$ and $\lambda_1 \geq 750$. Only one streamline per cell was allowed with a step size of 0.75 and a minimum length of $35mm$. The hyperstreamlines were colour mapped with the diffusion anisotropy.

The image indicates an approximately cylindrical anisotropy in most regions. Noticeable exceptions are the posterior limb of the internal capsule (5) and the splenium of the corpus callosum (4) where the minimum diffusivity is significantly reduced and the medium diffusivity is slightly reduced. As a result the diffusion anisotropy increases strongly. The colour coding of the streamlines in figure 7 and 8 indicates that mean diffusivity and diffusion anisotropy usually don't vary much even though the packing density in different white matter regions can vary by up to a factor of five ($60000 - 70000/mm^2$ in the pyramidal tract and $338000/mm^2$ in the corpus callosum [18]).

VI. Conclusion

Medical specialist are most familiar with slice images of raw data. Using an incremental approach starting with

colour mapped slices and extending to $2\frac{1}{2}$D and 3D techniques diffusion data can be systematically explored. New insight into diffusion tensor data is gained using barycentric colour maps which show the distribution of anisotropies over a region and indicate possible fiber tract crossing. A high amount of information can be encoded into a slice image using transparency modulated line integral convolution. The technique does not only indicates three dimensional fiber direction but also provides a visual segmentation of tissue types. A full 3D model of nerve fiber tracts is achieved by using streamtubes and hyperstreamlines. When using more advanced techniques parameter choice becomes increasingly important and care has to be taken when interpreting the visual results. Perception of 3D scenes can be improved by shaded 3D icons and by inserting anatomical structures into the scene.

We intend to use our visualization workbench for the exploration of various white matter diseases and hope to gain new insight into the progress of neurodegenerative diseases by employing the presented techniques.

VII. Acknowledgments

We would like to thank Peter J. Basser from the National Institute of Health, Bethesda, MD, for valuable discussions and Carlo Pierpaoli for providing us with the diffusion tensor data set of a healthy brain.

References

[1] P. J. Basser, J. Mattiello, and D. Le Bihan. MR diffusion tensor spectroscopy and imaging. *Biophysical Journal*, 66:259–267, 1994.

[2] Peter J. Basser. Inferring microstructural features and the physiological state of tissues from diffusion-weighted images. *NMR in Biomedicine*, 8(7-8):333–344, 1995.

[3] Peter J. Basser, Sinisa Pajevic, Carlo Pierpaoli, Jeffrey Duda, and Akram Aldroubi. In vivo fiber tractography using DT-MRI data. *Magnetic Resonance in Medicine*, 44(4):625–632, October 2000. URL: http://dir2.nichd.nih.gov/nichd/limb/stbb/invivofiber.pdf.

[4] Peter J. Basser and Carlo Pierpaoli. Microstructural and physiological features of tissues elucidated by quantitative-diffusion-tensor MRI. *Journal of Magnetic Resonance, Series B*, 111(3):209–219, 1996.

[5] Brian Cabral and Leith (Casey) Leedom. Imaging vector fields using line integral convolution. In James T. Kajiya, editor, *Computer Graphics (SIGGRAPH '93 Proceedings)*, volume 27, pages 263–272. ACM SIGGRAPH, Addison Wesley, August 1993.

[6] Thierry Delmarcelle and Lambertus Hesselink. Visualizing second-order tensor fields with hyperstreamlines. *IEEE Computer Graphics and Applications*, 13(4):25 – 33, 1993. URL: http://www.nas.nasa.gov/NAS/TechReports/RelatedPapers/StanfordTensorFieldVis/CGA93/abstract.html.

[7] Marjorie A. England and Jennifer Wakely. *A Colour Atlas of the Brain & Spinal Cord - An Introduction to Normal Neuroanatomy*. Wolfe Publishing Ltd., 2-16 Torrington Place, London WCIE 7LT, England, 1991.

[8] Arthur C. Guyton. *Basic Neuroscience - Anatomy and Physiology*. W.B. Saunders Company, 1987.

[9] Joseph Hanaway, Thomas A. Woolsley, Mokhtar H. Gado, and Jr. Melville P. Roberts. *The Brain Atlas*. Fitzgerald Science Press, Bethesda, Maryland, 1998.

[10] Maj Hedehus. Magnetic resonance diffusion tensor imaging. URL: http://www.stanford.edu/~majh/FAtheory.html.

[11] J. Robin Highley, Margaret M. Esiri, Brendan McDonald, Mario Cortina-Borja, Brian M. Herron, and Timothy J. Crow. The size and fibre composition of the corpus callosum with respect to gender and schizophrenia: A post mortem study. *Brain*, 122:99 – 110, 1999. URL: http://www.psychiatry.ox.ac.uk/powic/size_fibre_composition.html.

[12] M.D. Keith A. Johnson and J. Alex Becker. The whole brain atlas. URL: http://www.med.harvard.edu/AANLIB/home.html.

[13] Gordon Kindlmann and David Weinstein. Hue-balls and lit-tensors for direct volume rendering of diffusion tensor fields. In David Ebert, Markus Gross, and Bernd Hamann, editors, *Proceedings of Visualization '99*, pages 183 – 189. IEEE, October 1999.

[14] W. Michael Lai, David Rubin, and Erhard Krempl. *Introduction to Continuum Mechanics*, volume 17 of *Pergamon Unified Engineering Series*. Pergamon Press, Headington Hill Hall, Oxford OX3 0BW, England, revised edition in si/metric units edition, 1986.

[15] David H. Laidlaw, Eric T. Ahrens, David Kremers, and Carol Readhead. Visualizing diffusion tensor images of the mouse spinal cord. In David Ebert, Hans Hagen, and Holly Rushmeier, editors, *Proceedings of Visualization '98*, pages 127 – 134. IEEE, Computer Society Press, October 1998.

[16] Haim Levkowitz and Gabor T. Herman. Color scales for image data. *IEEE Computer Graphics and Applications*, 12(1):72 – 80, January 1992.

[17] Sharon Peled, Hákon Gudbjartsson, Carl-Fredrik Westin, Ron Kikinis, and Ferenc A. Jolesz. Magnetic resonance imaging shows orientation and asymmetry of white matter fiber tracts. *Brain Research*, 780:27 – 33, January 1998. URL: http://splweb.bwh.harvard.edu:8000/pages/papers/peled/html BrainRes.html.

[18] Carlo Pierpaoli, Peter Jezzard, Peter J. Basser, Alan Barnett, and Giovanni Di Chiro. Diffusion tensor MR imaging of the human brain. *Radiology*, 201(3):637 – 648, December 1996.

[19] C. Poupon, J.-F. Mangin, V. Frouin, J. Régis, F. Poupon, M. Pachot-Clouard, D. Le Bihan, and I. Bloch. Regularization of MR diffusion tensor maps for tracking brain white matter bundles. In William M. Wells, Alan Colchester, and Scott Delp, editors, *Medical Image Computing and Computer-Assisted Intervention - MICCAI '98*, Lecture Notes in Computer Science 1496, pages 489 – 498, Cambridge, MA, October 1998. Springer Verlag.

[20] Paul M. Thompson, Katherine L. Narr, Rebecca E. Blanton, and Arthur W. Toga. *Proceedings of the NATO ASI on the Corpus Callosum*, chapter Mapping Structural Alterations of the Corpus Callosum during Brain Development and Degeneration. Kluwer Academic Press, 2000. In Press, URL: http://www.loni.ucla.edu/~thompson/MarcoChpt/MarcoChpt_full.html.

[21] David Weinstein, Gordon Kindlmann, and Eric Lundberg. Tensorlines: Advection-diffusion based propagation through diffusion tensor fields. In David Ebert, Markus Gross, and Bernd Hamann, editors, *Proceedings of Visualization '99*, pages 249 – 253. IEEE, October 1999.

[22] C.-F. Westin, S. E. Maier, B. Khidir, P. Everett, F. A. Jolesz, and R. Kikinis. Image processing for diffusion tensor magnetic resonance imaging. In Chris Taylor and Alan Colchester, editors, *Medical Image Computing and Computer-Assisted Intervention - MICCAI '99*, Lecture Notes in Computer Science 1679, pages 441 – 452, Cambridge, UK, September 1999. Springer Verlag.

[23] C.-F. Westin, S. Peled, H. Gubjartsson, R. Kikinis, and F. A. Jolesz. Geometrical diffusion measures for MRI from tensor basis analysis. In *Proceedings of ISMRM, 5th meeting*, April 1997. URL: http://www.spl.harvard.edu:8000/pages/ppl/westin/papers/smr97/htmlversion.html.

[24] Mason Woo, Jackie Neider, and Tom Davis. *OpenGL Programming Guide*. Addison-Wesley Publication Company Inc., 3 edition, 1997.

[25] Burkhard C. Wünsche. *The Visualization of Tensor Fields in Biological Tissue*. PhD thesis, University of Auckland, 2001. (To be published).

[26] Burkhard C. Wünsche and Richard Lobb. A toolkit for the visualization of stress and strain tensor fields in biological tissue. In *Proceedings of VIP'99*, pages 6 – 15, 1999.

[27] Song Zhang, Charlie Curry, Daniel S. Morris, and David H. Laidlaw. Visualizing diffusion tensor MR images using streamtubes and streamsurfaces. URL: http://www.cs.brown.edu/~dhl/pdf/hbp00dti.pdf, 2000.